Doppler-Free Saturated Absorption Spectroscopy Lab Report

Björn Sumner and Benjamin Crane
13 Feb 2018

Motivation and Context

The atomic hyperfine structure arises from the interaction of the nuclear and electron magnetic moments. This structure is responsible for many technological achievements, including the development of atomic clocks. In fact, the SI second is defined by counting the number of transitions between two hyperfine states in the cesium 133 atom [1]. Additionally, the famous 21-cm line in astronomy is generated by a hyperfine transition in interstellar hydrogen[2].

The measurement of hyperfine splittings can be performed by using Doppler-Free Saturated Absorption Spectroscopy. We will use this technique to measure the splittings of several hyperfine structures of Rubidium.

Physics and Predictions

Atomic Spectra

Rubidium is a hydrogen-like atom with a single $5s^1$ electron in its outer shell. This electron gives rise to the two term states we will be interested in: $5^2\mathrm{S}_{1/2}$ and $5^2\mathrm{P}_{3/2}$. There are two naturally occurring isotopes of Rubidium: 72% abundant ^{85}Rb with spin number $I = 5/2$ and 28% abundant ^{87}Rb with $I = 3/2$. The Hamiltonian describing the atom is given by

$$H = \frac{p^2}{2m} - \frac{Z_{eff}e^2}{4\pi\epsilon_0 r} + \zeta(r)\vec{L}\cdot\vec{S} + \alpha\vec{J}\cdot\vec{I} + \frac{\beta}{2I(2I-1)J(2J-1)}\left[3(\vec{I}\cdot\vec{J})^2 + \frac{3}{2}(\vec{I}\cdot\vec{J}) - I(I+1)J(J+1)\right] \quad (1)$$

$\frac{p^2}{2m}$ contains the kinetic energy term and $-\frac{Z_{eff}e^2}{4\pi\epsilon_0 r}$ the standard Coulomb attractive potential. $\zeta(r)\vec{L}\cdot\vec{S}$ is the spin orbit coupling term, which gives rise to the broad term states such as $5^2\mathrm{S}_{1/2}$ and $5^2\mathrm{P}_{3/2}$. The transition between these states is 780 nm. The final two terms result from the hyperfine interaction. The former term is the hyperfine interaction between the magnetic dipole of the nucleus and electron, while the latter comes from the nuclear electric quadrupole. These two terms will produce the hyperfine states we will explore in this lab, and we label these states by their quantum number F, the magnitude of the total angular momentum $\vec{F} = \vec{J} + \vec{I}$. The possible quantum numbers vary from $|J - I|$ to $J + I$. These energy levels are shown in figure 1. In this lab, we will look at ^{85}Rb transitions from $5^2\mathrm{S}_{1/2}\,\mathrm{F} = 3$ to $5^2\mathrm{P}_{3/2}\,\mathrm{F'} = 1, 2, 3, 4$ and ^{87}Rb transitions from $5^2\mathrm{S}_{1/2}\,\mathrm{F} = 2$ to $5^2\mathrm{P}_{3/2}\,\mathrm{F'} = 0, 1, 2, 3$.

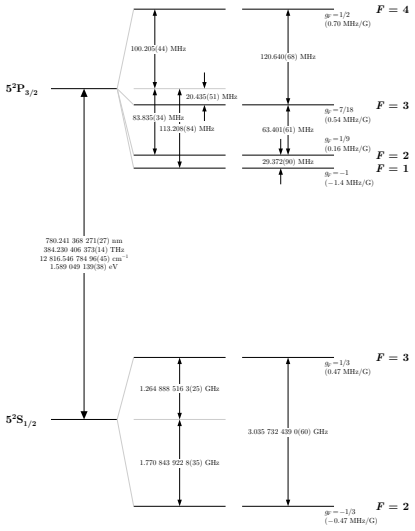

Figure 2: Rubidium 85 D_2 transition hyperfine structure, with frequency splittings between the hyperfine energy levels. The excited-state values are taken from [11, 26], and the ground-state values are from [26]. The relative hyperfine shifts are shown to scale within each hyperfine manifold (but visual spacings should not be compared between manifolds or to the optical splitting). The approximate Landé g_F-factors for each level are also given, with the corresponding Zeeman splittings between adjacent magnetic sublevels.

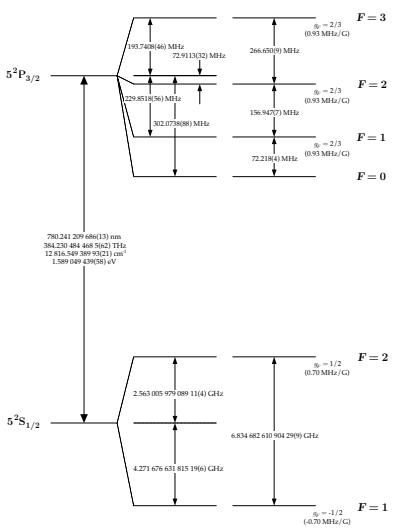

Figure 2: ^{87}Rb D_2 transition hyperfine structure, with frequency splittings between the hyperfine energy levels. The excited-state values are taken from [6], and the ground-state values are from [16]. The approximate Landé g_F-factors for each level are also given, with the corresponding Zeeman splittings between adjacent magnetic sublevels.

(a) ^{85}Rb[3] (b) ^{87}Rb[4]

Figure 1: Rubidium Energy Levels

By using the Hamiltonian of equation 1 in we can obtain the energies of the various hyperfine levels, and by dividing by Planck's constant, we can obtain an expression for the frequency associated with each level, indexed by quantum numbers J and F:

$$\nu_{J,F} = \nu_J + A\frac{C}{2} + B\frac{\frac{3}{4}C(C+1) - I(I+1)J(J+1)}{2I(2I-1)J(2J-1)}$$

where

$$C = F(F+1) - J(J+1) - I(I+1)$$

By using these formulas, we can obtain expressions in the unknown coefficients A and B for the 'absolute' frequencies, and average these levels to get the crossover 'absolute' frequencies. Once we have these six levels, we can take the differences to obtain expressions for the splittings. We can then use the results from our experiment to obtain values for A and B and compare them to the accepted values.

^{85}Rb $5^2P_{3/2}$ Frequencies

$F' = 4, J = \frac{3}{2}, I = \frac{5}{2}$

$$C = \frac{15}{2} \qquad \nu_{\frac{3}{2},4} = \nu_J + A\frac{15}{4} + B\frac{1}{4} = \nu_J + \frac{150A + 10B}{40}$$

$F' = 3, J = \frac{3}{2}, I = \frac{5}{2}$

$$C = -\frac{1}{2} \qquad \nu_{\frac{3}{2},3} = \nu_J - A\frac{1}{4} - B\frac{11}{20} = \nu_J - \frac{10A + 22B}{40}$$

$F' = 2, J = \frac{3}{2}, I = \frac{5}{2}$

$$C = -\frac{13}{2} \qquad \nu_{\frac{3}{2},2} = \nu_J - A\frac{13}{4} - B\frac{1}{10} = \nu_J - \frac{130A + 4B}{40}$$

Crossovers

$$\nu_{\bar{43}} = \nu_J + \frac{\nu_{\frac{3}{2},4} + \nu_{\frac{3}{2},3}}{2} = \nu_J + \frac{70A - 6B}{40}$$

$$\nu_{\bar{42}} = \nu_J + \frac{\nu_{\frac{3}{2},4} + \nu_{\frac{3}{2},2}}{2} = \nu_J + \frac{10A + 3B}{40}$$

$$\nu_{\bar{32}} = \nu_J + \frac{\nu_{\frac{3}{2},3} + \nu_{\frac{3}{2},2}}{2} = \nu_J - \frac{70A + 13B}{40}$$

We thus obtain the following splittings:

Splittings

$$\nu_4 - \nu_{\bar{43}} = 2A + \frac{2}{5}B \qquad \nu_{\bar{43}} - \nu_{\bar{42}} = \frac{3}{2}A - \frac{9}{40}B$$
$$\nu_{\bar{42}} - \nu_3 = \frac{1}{2}A + \frac{5}{8}B \qquad \nu_3 - \nu_{\bar{32}} = \frac{3}{2}A - \frac{9}{40}B$$
$$\nu_{\bar{32}} - \nu_2 = \frac{3}{2}A - \frac{9}{40}B$$

^{87}Rb $5^2P_{3/2}$ Frequencies

$F' = 3, J = \frac{3}{2}, I = \frac{3}{2}$

$$C = \frac{9}{2} \qquad \nu_{\frac{3}{2},3} = \nu_J + A\frac{9}{4} + B\frac{1}{4} = \nu_J + \frac{90A + 10B}{40}$$

$F' = 2, J = \frac{3}{2}, I = \frac{3}{2}$

$$C = -\frac{3}{2} \qquad \nu_{\frac{3}{2},2} = \nu_J - A\frac{3}{4} - B\frac{3}{4} = \nu_J - \frac{30A + 30B}{40}$$

$F' = 1, J = \frac{3}{2}, I = \frac{3}{2}$

$$C = -\frac{11}{2} \qquad \nu_{\frac{3}{2},1} = \nu_J - A\frac{11}{4} + B\frac{1}{4} = \nu_J - \frac{110A - 10B}{40}$$

Crossovers

$$\nu_{\bar{32}} = \nu_J + \frac{\nu_{\frac{3}{2},3} + \nu_{\frac{3}{2},2}}{2} = \nu_J + \frac{30A - 10B}{40}$$

$$\nu_{\bar{31}} = \nu_J + \frac{\nu_{\frac{3}{2},3} + \nu_{\frac{3}{2},1}}{2} = \nu_J - \frac{10A - 10B}{40}$$

$$\nu_{\bar{21}} = \nu_J + \frac{\nu_{\frac{3}{2},2} + \nu_{\frac{3}{2},1}}{2} = \nu_J - \frac{70A + 10B}{40}$$

We thus obtain the following splittings:

Splittings

$$\nu_3 - \nu_{\bar{32}} = \frac{3}{2}A + \frac{1}{2}B \qquad \nu_{\bar{32}} - \nu_{\bar{31}} = A - \frac{1}{2}B$$
$$\nu_{\bar{31}} - \nu_2 = \frac{1}{2}A + B \qquad \nu_2 - \nu_{\bar{21}} = A - \frac{1}{2}B$$
$$\nu_{\bar{21}} - \nu_1 = A - \frac{1}{2}B$$

Doppler Broadening

The spectra given in the previous section are obtained from a description of nature in the atom's frame of reference with no external effects. However, real Rubidium atoms are subject to thermal motion, and as such these spectral lines will undergo broadening owing to the motion of the atoms relative to the laser. Atoms moving toward the laser will 'see' radiation blueshifted, and so absorption will only occur if the incoming photons are of a lower frequency than predicted by the spectra in figure 1. Similarly, atoms moving away from the laser will absorb photons of higher frequency. Because the velocity of these atoms follows the Maxwell distribution, it can be expected that the spectral lines will similarly follow such a distribution. It can be shown that the half width of these distributions is given by

$$\Delta\nu_{1/2} = 2\frac{\nu_0}{c}\sqrt{\frac{2kT}{M}\ln(2)} \tag{2}$$

where ν_0 is the rest frame atomic resonance, M is the mass of the atom and T is the temperature of the sample.

We can use this to predict the expected half width of the D2 lines. Using figures from Steck[3][4],

^{85}Rb D_2

$$\begin{aligned}\Delta\nu_{1/2} &= \frac{2}{\lambda_0}\sqrt{\frac{2kT}{M_{85}}\ln(2)} \\ &= \frac{2}{780.241\,\text{nm}}\sqrt{\frac{2\left(1.381\times10^{-23}\,\frac{\text{J}}{\text{K}}\right)(293\,\text{K})}{1.410\times10^{-25}\,\text{kg}}\ln(2)} \\ &\approx 511\text{MHz}\end{aligned} \tag{3}$$

^{87}Rb D_2

$$\begin{aligned}\Delta\nu_{1/2} &= \frac{2}{\lambda_0}\sqrt{\frac{2kT}{M_{87}}\ln(2)} \\ &= \frac{2}{780.241\,\text{nm}}\sqrt{\frac{2\left(1.381\times10^{-23}\,\frac{\text{J}}{\text{K}}\right)(293\,\text{K})}{1.443\times10^{-25}\,\text{kg}}\ln(2)} \\ &\approx 505\text{MHz}\end{aligned} \tag{4}$$

These broadened spectra mask the hyperfine structure of the atoms, and so we must use Doppler-Free Saturated Absorption Spectroscopy to tease out these individual spectra.

Doppler-Free Saturated Absorption Spectroscopy

To isolate the hyperfine structure, we use saturation absorption spectroscopy. When a probe beam passes through the rubidium sample, thermal motion of the atoms will result in absorption of this beam across a range of frequencies, as these frequencies will be blue-shifted

or red-shifted to the atomic resonance owing to the motion of the atoms relative to the probe source. However, if we were to use a strong pump beam to saturate the absorption across the entire frequency range, then both beams will be on resonance at the transition frequency for a subpopulation of the atoms that have velocities perpendicular to the propagation direction of the lasers. These atoms can then undergo *stimulated* emission from the probe beam, and thus the absorption will be reduced (the photodetector will register a stronger signal) at the transition frequency. By using an additional probe beam separate from the overlap, we can subtract the signals to obtain the Doppler-free saturated absorption signal.

As an added bonus, this strong pump beam also favors the higher ground state in both isotopes ($F = 3$ for ^{85}Rb, $F = 2$ for ^{87}Rb), which promotes the D_2 line we are interested in observing.

Michelson Interferometer

Though we can obtain a plot of voltage against time, we must have a way of comparing the time differences in the signals to an associated frequency. We can use a Michelson interferometer to calibrate our signal. By precisely measuring the different leg lengths of the interferometer, then a time-varying frequency of light entering the interferometer will produce a time-varying intensity of its recombined beams. It can be shown that the frequency spacing of the interference maxima is given by

$$\Delta\nu = \frac{c}{2\Delta L} \tag{5}$$

Thus, by using the period of the interferometer signal which is associated with a frequency span, we have a way of measuring the frequency spacings of interest from the spectroscopy signals.

Experiment and Data

Experimental Setup

We designed the experimental setup on the optical table to accommodate both Doppler-Free Saturated Absorption Spectroscopy and the Michelson Interferometer for calibration. Using the infrared camera and the handheld cardviewer allowed us to trace the paths of laser beam. The laser was directed through a cube beam splitter with one path continuing towards the Michelson Interferometer setup, and the other towards a thick beam splitter. The thickness of the beam splitter allows for spatially separated but parallel beams directly through the Rubidium vapor sample. These two weak beams are called the reference probe beam and the overlapping probe beam. The main portion of the laser continued straight through the thick beam splitter, becoming the start of the pump beam. The strong pump beam was angled with a mirror towards the opposite end of the table and was then angled with a separate mirror to overlap a probe beam. These two beams are propagating in opposite directions. The overlapping probe beam continues through the rubidium vapor sample and is then directed with a mirror onto the photodetector. The reference probe beam is also

reflected from a mirror through an optical attenuator and onto a separate photodetector. To achieve comparable power from the two probe beams we used a translation stage holding the variable attenuator to reduce the intensity of the reference beam. This was done visually with the aid of the oscilloscope displaying the two channels of the photodetectors.

The beam passing through the first beam splitter is incorporated into the Michelson Interferometer. This interferometer consists of a thin microscope slide at $\approx 45°$ to act as a 50-50 beam splitter. The longer reflected leg of the Michelson Interferometer has a measured length of 388.5 $\pm$0.5 mm, while the shorter leg is measured to have a length of 94.5 $\pm$0.5mm. The laser traveled down and back each leg of the Michelson Interferometer and recombined at the beam splitter before continuing to the photodetector. We ensured the beams were parallel and occupying the same space by using a card to ensure there was no divergence from the recombination point to the far wall approximately 3 meters away. After orienting the mirrors, beam splitters and photodetectors we noticed an odd feedback signal superimposed on both probe signals on our oscilloscope. After discussing the feedback with Professor Jun Ye, we were able to determine the feedback was a result of the interferometer beams entering into the spectroscopy component of the table. To negate these effects we installed another variable optical attenuator at an angle between the cube splitter and microscope slide to prevent the interferometer signal from entering the spectroscopy setup. This eliminated the anomalous addition from the probe beam signals. Using the Math function of the oscilloscope we were able to subtract the Doppler-broadened spectral lines with hyperfine structure (overlapping probe) from the Doppler-broadened spectral lines (reference probe) we were able to display just the specific peaks of the hyperfine structure. See figure 2 for a picture of our optical table.

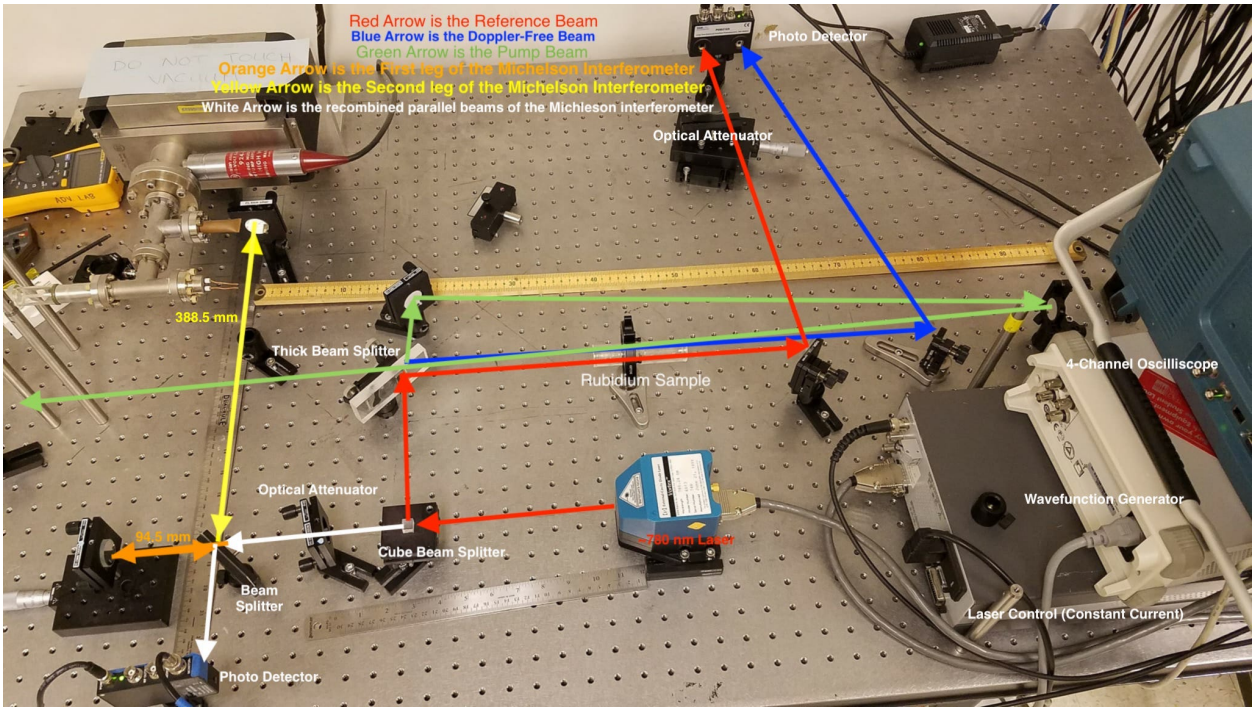

Figure 2: Experiment Layout

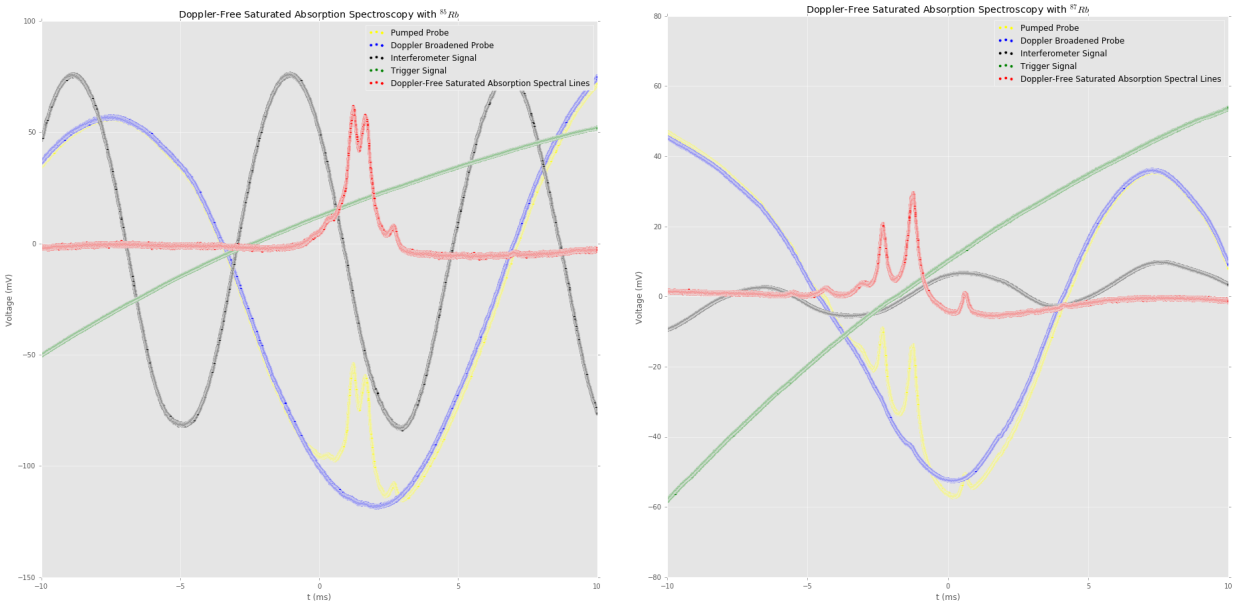

(a) ^{85}Rb (b) ^{87}Rb

Figure 3: Rubidium D_2 Oscilloscope Data

Toggling the Vortex Laser controls for the voltage and the wave-function generator's frequency and peak-to-peak ramp voltage allowed for panning left and right and zooming in and out on specific portions, focusing on the hyperfine splitting of the $5^2P_{3/2}$ states. We decided to arrange the output from the Michelson Interferometer to be displayed along side the three other signals, allowing for a direct comparison. These signals included the reference probe beam, the pump-overlapped probe beam, the interferometer signal and the ramp voltage signal upon which the oscilloscope is triggered. By incorporating all of the signals onto the same oscilloscope we were able to directly compare all signals.

This allowed us to measure the full width at half maximum (FWHM) of the doppler broadened lines of both isotopes as well as the separation of the hyperfine states for the D_2 lines of both isotopes. We then were able to solve for the constants A and B of the $5^2P_{3/2}$.

A critical feature of our setup was the careful alignment of the pump beam. By ensuring the maximum overlap of the pump beam with one of the probe beams, we maximized the population in the higher ground states as well as the population of atoms interacting simultaneously with both pump and probe beams. This optimizes the amount of stimulated hyperfine transitions that occur, making our signals much clearer.

Results

Two representative sets of data for the D_2 transitions for both ^{85}Rb and ^{87}Rb are shown in figure 3.

As can be seen from figure 3, we were able to isolate 4 of the 6 D_2 hyperfine transitions (3 transitions, 3 crossovers) for ^{85}Rb, but all 6 D_2 transitions for ^{87}Rb.

We first obtain our 'meterstick' for measuring frequency spacings. To do this, we curve fit the interferometer signal to a cosine, and obtain a fitted period, δt. We then compare

spacings relative to this 'meterstick' by observing that the ratio of the frequency spacing we desire, f to the interferometer frequency spacing $\Delta\nu$ must equal the ratio of the time-spacing between the signals of interest τ to the time spacing of the interferometer period Δt:

$$\frac{f}{\Delta\nu} = \frac{\tau}{\Delta t}$$

By using equation 5, we obtain:

$$f = \frac{c}{2\Delta L \Delta t}\tau \tag{6}$$

By performing the curve fitting mentioned above, we find

We would like to measure the FWHM of the Doppler broadened D_2 transition. We do this by fitting the Doppler broadened probe signals to Gaussians, and then using the relation $FWHM = 2\sqrt{2\ln(2)}\sigma$, where σ is the standard deviation of the fitted Gaussian.

Error Analysis

Conclusions

References

[1] National Institute of Standards and Technology. *"Definitions of the SI base units"*, 2015.

[2] Green Bank Observatory. *"Prediction of 21cm line radiation"*.

[3] Daniel A. Steck. Rubidium 85 data. 2003.

[4] Daniel A. Steck. Rubidium 87 data. 2003.